Published in final edited form as:
Nat Struct Mol Biol. 2013 April ; 20(4): 454–460. doi:10.1038/nsmb.2530.

Structure of Active, Dimeric Human Telomerase

Anselm Sauerwald[1,2,*], **Sara Sandin**[1,3,*], **Gaël Cristofari**[2,†], **Sjors H.W. Scheres**[1], **Joachim Lingner**[2], and **Daniela Rhodes**[1,3]

[1]Medical Research Council Laboratory of Molecular Biology, Hills Road, Cambridge CB2 0QH, United Kingdom. [2]Swiss Institute for Experimental Cancer Research (ISREC), School of Life Sciences, Frontiers in Genetics National Center of Competence in Research, Ecole Polytechnique Fédérale de Lausanne (EPFL), 1015 Lausanne, Switzerland. [3]School of Biological Sciences, Nanyang Technological University, 60 Nanyang Drive, SBS-01s-45, Singapore 637551

Abstract

Telomerase contains a large RNA subunit TER and a protein catalytic subunit TERT. Whether telomerase functions as monomer or dimer has been a matter of debate. Here we report biochemical and labeling data that show that *in vivo* assembled human telomerase contains two TERT subunits and binds two telomeric DNA substrates. Importantly, catalytic activity requires both TERT active sites to be functional, demonstrating that human telomerase functions as a dimer. We also present the three-dimensional structure of active, full-length human telomerase dimer, determined by single-particle electron microscopy in negative stain. Telomerase has a bilobal architecture, with the two monomers linked by a flexible interface. The monomer reconstruction at 23Å resolution, and fitting of the atomic structure of the beetle TERT subunit reveals the spatial relationship between RNA and protein subunits, providing insights into the telomerase architecture.

Introduction

Telomeres, the protein/DNA complexes that cap the ends of eukaryotic chromosomes are essential for genomic stability and cell viability[1]. In eukaryotes, telomere length is maintained by the telomerase enzyme, a specialized reverse transcriptase capable of de novo DNA synthesis. Telomere maintenance in the majority of cancer cells involves the activation of telomerase[2]. Originally discovered by Greider and Blackburn in 1985 in the ciliate *T. thermophila*[3], the telomerase enzyme consists of an RNA subunit TER that contains an internal template for telomeric DNA-repeat synthesis[4] and a protein subunit TERT that contains a reverse transcriptase domain that catalyzes nucleotide addition[5,6]. The telomerase is a processive enzyme: In the first step of G-overhang synthesis, the 3′ end of the telomeric primer, the G-overhang, is positioned in the active site of the telomerase forming base pairs with the alignment region of the RNA template. In a second elongation step, nucleotide addition takes place to synthetize the telomeric DNA repeat, and in a third step the telomerase translocates to restart telomere repeat synthesis[7]. To accomplish all these

Correspondence and requests for materials should be addressed to: joachim.lingner@epfl.ch and rhodes@mrc-lmb.cam.ac.uk.
*These authors contributed equally to this work.
†Present address: University of Nice - Sophia-Antipolis, 06107 Nice Cedex 2, France.

Author contributions A.S. designed and carried out all the biochemical work and contributed to image processing. S.S. collected EM data and solved the structures. G.C. developed the super-telomerase cells. S.H.W.S designed and contributed to the structure refinement. J.L. and D.R. designed and supervised the project. All authors contributed to the writing of the paper.

Author Information The authors declare no competing financial interests.

Europe PMC Funders Author Manuscripts

catalytic steps, the telomerase enzyme would likely have to undergo substantial conformational changes.

Together TER and TERT form a tight complex that is sufficient for telomeric DNA repeat synthesis *in vitro*[8], whilst accessory proteins involved in assembly and localization have been found associated with the telomerase holoenzyme isolated from cells[9-12]. Whether human telomerase functions as a monomer[13] or a dimer[10,14-17] is a matter of debate[10,18]. *In vitro* reconstitution experiments demonstrated that telomerase contains two telomerase RNA moieties[14]. However, it was suggested that *in vitro* reconstitution may lead to formation of non-native multi-subunit complexes and that *in vivo* assembled human telomerase was monomeric[13].

A full understanding of telomerase function requires information on the three-dimensional structure of the telomerase. This has been hindered by the difficulty in obtaining sufficient quantities of purified, active and full-length telomerase complex. Therefore, in contrast to other important enzymes, such as the ribosome and RNA/DNA polymerases, knowledge of the telomerase structure has been limited to subdomains of the TER and TERT subunits[19-21]. Amino acid sequence analysis and mutational studies have established that the TERT subunit contains three domains: an N-terminal G-overhang binding (TEN) domain, the RNA binding domain (TRBD) and a C-terminal domain consisting of the reverse transcriptase (RT) domain (Fig.1a)[7,20].The most comprehensive structural information on the TERT subunit comes from the crystal structure of the beetle *T. castaneum* TERT in complex with a short DNA/RNA helix[22,23] confirming a structural conservation with other RTs such as HIV RT[24] and revealing the relative location of the TRBD with respect to the RT domains within TERT[25]. This beetle TERT subunit lacks the TEN domain present at the N-terminus of most TERTs, including hTERT, but the structure of this domain is known from the crystal structure of the isolated TEN domain of the ciliate *T. thermophila*[26].

Although the length of the RNA subunit is less well conserved than the protein subunit (from 147 nucleotides in protozoa to almost 2000 nucleotides in budding yeasts), phylogenetic and functional studies have revealed that all TERs contain two conserved structural elements: the catalytically essential pseudoknot/template core domain and a stem terminus element called CR4/CR5 in vertebrates[27], both of which have been shown to interact with TERT[28,29]. Structural information on the TER subunit is restricted to isolated segments of the RNA, including the functionally important pseudoknot[21]. Despite the structural information on TER and TERT sub-domains, little is known about the overall structure of human telomerase and how the various domains contribute to the architecture of full-length telomerase to form a functional enzyme. Here we present the first three-dimensional structural analysis of active, full-length human telomerase by single particle electron microscopy which reveals a dimeric bilobal structure, as well as experimental evidence that the two TERT subunits in the telomerase dimer cooperate in catalytic activity.

Results

In vivo assembled human telomerase is a dimer

To obtain sufficient quantities of purified, active human telomerase for structural analyses, we made use of HEK293T ‘super-telomerase’ cells which over-express hTER and hTERT from transiently transfected plasmid constructs[30], and have 200-fold higher telomerase activity than untransfected HEK293T cells[31]. The purification exploits the protein-A tag cloned at the N-terminus of hTERT, followed by affinity chromatography and sucrose gradient fractionation. To facilitate the tracking of the telomerase in the sucrose gradient, the telomerase was incubated with a [^{32}P] 5′ labeled G-overhang oligonucleotide (5′-(TTAGGG)$_2$-3′) prior to the sedimentation. Figure 1b shows a well resolved peak that

sediments in the same position as the 670 kDa thyroglobulin size marker analysed in a parallel sucrose gradient (fig. S1c). Furthermore, tracking of the telomerase using a direct telomerase activity assay [10] shows that the peak of activity coincides with the position of the 670 kDa peak in the sucrose gradient (Fig. 1b. and 1c). The purified telomerase sample was further analysed for protein content by SDS-PAGE, which shows a band with the MW of hTERT (fig. S1a). Incubation of purified telomerase with 5′ [32P] labeled G-overhang oligonucleotide (5′-(TTAGGG)$_3$-3′) followed by native PAGE shows that the telomerase complex migrates as a very tight band, and hence is of homogeneous MW (fig. S1b). The composition of the purified telomerase sample was analysed by mass spectroscopy. This analysis (table S1) reveals that the purified telomerase contains the hTERT subunits and two accessory proteins, Nop10 and dyskerin[32]. In conclusion, our data show that the purified human telomerase is active and that both the G-overhang bound and unbound telomerase complexes have a molecular weight consistent with that of a dimer consisting of two hTERT (127 kDa) and two hTER (153 kDa) subunits, as well as the two accessory proteins Nop10 (7.7 kDa) and dyskerin (58 kDA). This observation is in agreement with findings from a previous purification of the human telomerase complex from untransfected HEK239T cells[10].

Figure 1D shows an electron micrograph of purified, *in vivo* assembled human telomerase bound to the G-overhang oligonucleotide 5′-(TTAGGG)$_2$-3′. Inspection of the micrograph shows side views of many particles with a bilobal structure. Two- and three-dimensional structural information was obtained by single particle classification (Fig. 1e) and electron tomography (Fig. 1f) respectively (For image processing procedures, see Supplementary Material). These analyses reveal that the telomerase enzyme has an elongated structure, 280 Å in length and 125 Å in width, consisting of two spherical lobes connected by a region of thin density. The size of the telomerase particle is consistent with the estimated molecular weight (670 kDa) and the distribution of density into two lobes of similar size suggests the presence of a homodimeric complex. To establish whether the telomerase complex can bind one or two telomeres, a purified telomerase preparation was incubated with a G-overhang oligonucleotide 5′-(TTAGGG)$_2$-3′ labeled at its 5′ end with biotin and 5nm colloidal gold coated with monovalent streptavidin[33]. Colloidal gold can clearly be recognized as 5nm black dots bound to telomerase dimers (Fig. 1g, encircled), whereas excess monodisperse gold have a thin streptavidin coat (Fig. 1g, arrows). No particles resembling telomerase could be detected in a control sample containing streptavidin gold (Fig. 1h). Out of 450 telomerase dimers analyzed, 13.5% had no gold bound, 50% had one gold particle bound and 36.5% had two gold particles bound. This analysis suggests that one dimeric telomerase particle can bind up to two G-overhang substrates. This in turn is consistent with the presence of two RNA templates, and hence two TER subunits per telomerase complex.

Telomerase is a functional dimer

To address the question of whether active human telomerase contains one or more hTERT subunits, the telomerase enzyme was assembled *in vivo* from differently tagged TERT subunits. Expression plasmids of WT-hTERT containing either a N-terminal 13×Myc or an N-terminal ZZ(=2-protein A-tags)_(TEVsite)_3×Flag tag were generated and the two plasmids were co-expressed at a ratio of 1:1 or 1:6 together with hTER in HEK293T cells as described above. The differential tagging not only permits affinity *purification*, but results in TERT subunits of different MWs, which permits unambiguous interpretation of the composition of the *in vivo* assembled telomerase. Firstly, western blot analysis of cell lysates using an affinity purified polyclonal antibody against the C-terminus of hTERT, shows that the differently tagged TERT subunits are expressed in approximately the ratios expected from the input plasmid concentrations (Fig. 2a, Lanes 3 and 5 and fig.S2a-b). Secondly, the composition of telomerase complexes was investigated by binding ZZ-tagged

hTERT to IgG sepharose followed by TEV protease cleavage of the TEV site present in the ZZ-tagged hTERT subunit only. Western blot analysis of the released immunoaffinity purified complexes shows that 13×Myc_hTERT co-purifies with ZZ-tagged hTERT (Fig. 2a, Lanes 7 and 9), whilst in the absence of co-expressed ZZ-tagged hTERT, 13×Myc_hTERT does not bind to IgG sepharose (fig. S2 c-d, Lane 6). Furthermore, the intensity of the bands in the western blot (Fig. 2a, Lanes 7 and 9) is consistent with TEV cleavage releasing 3×Flag_hTERT homodimers and 3×Flag_hTERT/13×Myc hTERT heterodimers in the appropriate concentrations (as determined by the expression plasmid ratios) (Fig. 2a). Thus, the 13×Myc_hTERT subunit must have been in complex with the ZZ-tagged hTERT subunit to co-purify in the immunoaffinity purification. This result provides strong evidence that two TERT subunits are present per human telomerase complex and is consistent with both the G-overhang binding data (Fig. 1g) and the molecular weight estimation of purified telomerase (Fig. 1b).

We next asked whether the two TERT subunits in a telomerase complex function independently of each other, or whether they cooperate for catalytic activity. For this analysis we generated a catalytically dead active site mutant (V709A, D710I) [34]: (DN)-ZZ_(TEVsite)_3×Flag_hTERT (fig. S2a-b, Lane 4). This mutant, or the corresponding wild type (WT)-ZZ_(TEVsite)_3×Flag_hTERT were co-expressed with (WT)-13×Myc_hTERT at plasmid ratios of 1:1 or 6:1. The western blot analysis (Fig. 2a, Lanes 2 to 5) shows that the WT/DN TERT subunits are expressed in the expected ratios. To test whether TERT subunits function independently or cooperate, telomerase complexes were affinity purified via the ZZ-tag and complexes released by TEV cleavage as described above (Fig. 2a, Lanes 6 to 9). Thus, with the (DN) ZZ-tagged hTERT mutant, the complexes released contain WT hTERT only as DN/WT heterodimer, but not as WT/WT homodimers (Fig. 2a, Lanes 6 and 8). Significantly, quantification of telomerase catalytic activity, by both the telospot and direct telomerase activity assays[14] (Fig. 2b-c, Lanes 6 and 8), reveal that the telomerase complexes containing a mixture of catalytically inactive and catalytically active hTERT are totally catalytically inactive for both repeat addition processivity and nucleotide addition processivity (Fig. 2c, Lanes 6 and 8) (see fig. S2 c-d, Lanes 2 to 5, 7 and 8 for quantification). In contrast, the WT/WT TERT containing complexes are active as expected (Fig. 2b-c, Lanes 7 and 9). Therefore, the presence of a catalytically inactive TERT subunit in the telomerase complex has a dominant-negative impact on catalytic activity. These results establish that the human telomerase not only is structurally a dimer, but that telomerase activity requires the cooperation between the two TERT subunits in a dimer.

3-D reconstruction of the telomerase dimer

For single particle EM analysis of the telomerase dimer bound to the G-overhang oligonucleotide 5′-$(TTAGGG)_2$-3′, the sucrose gradient fractionation described above (Fig. 1b) was carried out in the presence of 0 to 0.1% glutaraldehyde (GraFix)[35]. This gentle cross-linking method has previously been demonstrated to improve structural homogeneity, particularly for low-abundance complexes that may otherwise dissociate during the preparation of EM grids. Importantly, parallel sucrose gradient fractionations of purified telomerase samples in the presence or absence of glutaraldehyde, show the same sedimentation profile (Fig. 1b). This indicates that the cross-linking did not effect the structural composition and that the cross-linked telomerase sample represents the active conformation of the enzyme (Fig. 1c). After the sucrose gradient fractionation, the concentration of the purified telomerase was very low and this precluded 3D structure determination by cryo EM. After concentrating the sample onto a freshly prepared carbon coated grid (Supplementary Material), we could detect 30-100 particles/image plate which was sufficient for single particle analysis by negative stain.

Figure 3a shows a representative field-view of the raw telomerase particles in negative stain, in which top views and side views of the telomerase dimer can clearly be recognized. A data set containing 20,127 telomerase particles was subjected to 2D class averaging by reference-free procedures using ~200 images/class (For image processing procedures see Supplementary Material). Figure 3b-d shows a gallery of 2D class averages representing top views (Fig. 3b), tilted views (Fig. 3c) and side views (Fig. 3d). Figure 3e shows two representative class average side views after they have been rotationally aligned, displaying a bilobal structure in which the two lobes are connected by a thin region of density. One of the two lobes has a V-shaped opening (Fig. 3e-f indicated with a **) and the other appears closed (Fig. 3e-f, indicated with a *). Inspection of the rotationally aligned class averages revealed similar monomer densities, however the relative orientation of the monomers in the dimer differ. The difference detected is illustrated by a simple movie composed of these two 2D class averages in sequence (Fig. 3e, Supplementary movie S1). This analysis suggests that telomerase has a flexible dimer interface that could act as a hinge region.

In addition to 2D classification, the 3D structure of the telomerase dimer was refined using the low-resolution subtomogram average (shown in Fig. 1f) as a reference model for 3D single particle refinement (Online Methods). Distinct conformations were further classified by three-dimensional maximum-likelihood analysis in Fourier space (MLF3D)[36]. After 25 rounds of non-supervised angular refinement, four reconstructions (Fig. S3c-f) were calculated and the absolute hand and the overall correctness of the dimer structure were assessed using a modified version of tilt-pair validation method[37] (Fig. S4). Figure 3f shows different orientations of a representative density map calculated from a sub-population of 3,659 particles at a resolution of 30 Å. Top views, tilted views and side views of the dimer density agree well with independently obtained reference-free 2D class averages in Figure 3b-e. These features include a characteristic V-shaped opening in one of the monomers, whilst the other is more closed. From the location of the nano-gold labelled G-overhang we can calculate that the distance between the two catalytic pockets in a telomerase dimer is 180-190Å (Fig. 3g). To test whether the difference in monomer conformation observed was due to sub-saturated levels of bound G-overhang oligonucleotide, we repeated the 2D classification (as described above) of a telomerase prepared in absence of DNA. No difference could be detected between class averages of telomerase in the presence (Fig. 3b) or absence of bound DNA (data not shown) indicating that the conformation of the monomers as well as the flexibility of the dimer interface is independent of G-overhang binding. In summary, the 3D structural determination of the telomerase dimer establishes that the two monomers in the dimer have different conformations, one open and one closed, and are linked by a flexible dimer interface (Fig. 3h). Future analyses will be required to establish the role of the telomerase structure dynamics in the binding of two telomere substrates and telomeric DNA synthesis.

Independently refined monomers and composite dimers

To circumvent refinement problems arising from the flexibility in the telomerase dimer interface, we processed the two halves of the telomerase dimer independently. From each class average of the telomerase dimer (excluding top views), the centre of each monomer was measured manually and the corresponding centres in the raw image stack were calculated. Next sub-images were boxed out as shown in Figure 4a, keeping images corresponding to the open V-shaped monomer separate from the closed monomer. The 3D refinements were carried out by MLF3D as described above. As expected, the resolution of the monomer structures markedly improved: measuring 23 Å for the open monomer and 21 Å for the closed. Although of similar resolutions, the V-shaped open monomer density had more clearly defined density distribution as can be explained by alignment procedures that, in general, work better with pronounced features. The dimer interface was not refined using

this procedure and therefore has been removed from side views shown in Figure 4b. Next, the independently refined 3D-monomer reconstructions were re-assembled into composite dimers based on the angles previously measured in the individual 2D class averages. The composite dimer shares many structural features with the density calculated for the telomerase dimer, but are better resolved (Compare Fig 3f. and Fig 4d.). Figure 4c shows a comparison of three 2D class averages, the corresponding composite 3D-reconstruction and projections of composite dimers. The close similarity between features in the 3D EM density of composite dimers and the 2D class averages indicates that the open and closed monomers were well refined.

The open monomer reconstruction shows several distinct features that allowed the fitting of the atomic structure of the beetle TERT subunit[22,25] into the EM density (Fig. 5a-c). This was done using an automatic six dimensional search in real space, for which only one solution was obtained. The excellent fit is supported both by the similarity in the overall shape of the protein subunit and by the coincidence of the catalytic core channel in the crystal structure with a channel in the EM density (Fig. 5c). These features can also be recognized in the crystal structure of the beetle TERT after filtering to 20Å resolution (Fig. S5b). To validate our assignment of the TERT subunit to the correct region of the EM density map, we first tested different antibodies to pinpoint the protein subunit. Although we could detect binding, the EM images were not informative as the molecular weight of IgG is the same MW range as the TERT subunit. Instead, we produced and purified telomerase (as described above) in which the TERT subunit contained an N-terminal 6×His-tag (ZZ_(TEV)_6×His_5x(AAAKE) ~37Å long alpha Helix_3x_Flag_hTERT). The location of the His-tag was found by using Ni-NTA coated 5nm colloidal gold. Visual inspection of particles showed that the majority of the gold particles were located at the periphery of the telomerase dimer (Fig. 5d). To obtain the distribution of the location of the gold particles in the telomerase dimer, we measured the distance from the centre of 100 gold particles to the dimer interface. The plot in Fig. 5e shows a pronounced peak at 110Å distance, which is in good agreement with the fitted location of the TERT subunit in the EM density of the “open” monomer (Fig. 5a-c).

Discussion

The determination of the first 3D-structure of active, full-length human telomerase assembled *in vivo* shows that it has a bilobal architecture (Fig. 1d-f and Fig.3) and a molecular weight consistent with a dimeric complex (Fig. 1b, fig. 1aS). These data together with our biochemical data provide strong evidence that the bilobal structure arises from the presence of two TERT subunits, and two TER subunits (Fig. 1 and Fig. 2) and is able to bind two telomeric G-overhang substrates (Fig. 3g and h). For the TERT subunit, the excellent fit of the crystal structure of the beetle TERT subunit (ref 23-24) into the EM map reveals the location of the RNA binding TRBD and catalytic RT domains within TERT (Fig. 5 a-c). We also demonstrate that for *in vivo* assembled telomerase, catalytic activity requires the cooperation between two TERT subunits in the telomerase dimer and that a catalytic pocked mutation in one of the two TERT subunits is dominant negative (Fig. 2). These observations substantially strengthen our previous conclusions derived from *in vitro* assembled telomerase where an RNA template mutant interfered with wild-type template function when co-assembled into telomerase particles[14]. They are also in agreement with MW estimations by others[10,38]. However, our results are in disagreement with publications in which it was concluded that human telomerase is monomeric[13,39]. Our work also underlines the importance of revisiting the conclusion that short telomere disease-associated telomerase mutations are not dominant-negative[13].

Why should telomerase function as a dimer? Our work demonstrates that a human telomerase dimer contains two catalytic pockets, located about 180 Å apart (corresponding to about a stretch of 50 nucleotides), that can associate with two telomeric DNA substrates (Fig. 3g and h). This suggests that telomerase may function by extending two telomeric ends in parallel. Interestingly, it has been demonstrated recently that the cohesion of replicated telomeres is important for telomere maintenance by telomerase, a function that is defective in dyskeratosis congenita-associated mutations in TIN2[40]. Therefore, an attractive hypothesis is that telomerase dimers extend aligned sister telomeres in parallel. This mechanism could enable sister telomeres to maintain equal lengths after extension. On the other hand, our data showing that the two TERT subunits in a telomerase dimer co-operate in telomerase activity could also have been explained with a mechanism in which telomerase binds and extends a single DNA substrate in a processive manner, as has been suggested from studies using partly purified Euplotes telomerase[41]. The observed flexibility of the interface between the two monomer lobes in the telomerase structure (Supplementary movie S1) could be functionally important by providing a hinge mechanism for the intramolecular translocation of the DNA substrate from one catalytic pocket to the other, as has been reported for other DNA/RNA polymerases such as the eukaryotic primosome[42]. However, since the DN/WT telomerase heterodimers were inactive even for the first round of telomeric DNA synthesis (Fig. 2c), which according to the translocation model should not require two active sites, we favour the parallel extension model.

The identification of the location of the TERT subunit in the EM density (Fig. 5 a-c) provides important insights into the domain organization of the telomerase dimer. First of all, the TERT subunit is located at the periphery of the open monomer, where it is separated from the rest of the complex by the V-shaped opening in the EM density. Because the fitted crystal structure of the beetle TERT subunit[22] corresponds to two thirds of hTERT, the majority of the EM density that is not occupied by the TERT subunit has to correspond to RNA, i.e. the hTER subunit. This interpretation agrees with the observation that the EM map in that region consists of three continuous regions of tubular density with diameters of 20-30Å (Fig. 5a-c), which is an expected feature of RNA helices (fig. S5a). This interpretation of the telomerase architecture implies that the dimer interface involves RNA-RNA interactions, which is in agreement with previous results[43] (Fig. 5F). However, we failed to dissociate dimeric TERT into monomers by RNase treatment (data not shown) and therefore we cannot exclude the involvement of some telomerase accessory protein in the formation of the dimer interface. Because the crystal structure of the beetle TERT subunit was solved in complex with a short DNA/RNA helix[23], its fitting into the EM density also pinpoints the location the 3′end of the G-overhang in the catalytic pocket of the RT domain (Fig. 5F). The consequence of this fitting is that the 5′end of the G-overhang points towards the centre of the monomer and a continuous region of density in its vicinity that we have tentatively assigned to the TER subunit (fig. S5), and suggests that the DNA binding TEN domain would be located adjacent to TRDB domain (Fig. 5F) consistent with the TERT domain structure (Fig. 1a). Furthermore, the fitting of the TERT subunit structure into the EM density map of the telomerase dimer reveals that the two catalytic pockets in a telomerase dimer (Fig. 3g-h and Fig. 5 d-e) and 6) are located very far apart, at a distance of 180-190 Å from each other. It will be interesting to unravel the mechanism by which they cooperate for telomerase activity, and indeed whether this distance is required to accommodate to telomeric ends in parallel.

Future work will aim at improving the resolution of the telomerase structure in order to reveal the fold of the telomerase RNA and its specific interaction with the various TERT domains as well as how the different conformational states we observe may be related to different functional states of the telomerase catalytic cycle. This study also provides the

starting point for investigating the structural basis of telomerase dimerization and its significance for catalysis and function.

Online Methods

Telomerase expression and purification

The telomerase complex was over-expressed using HEK293T cells[1] transiently transfected with hTERT- and hTER-expressing plasmid DNA (pVan145 [pCDNA6-ZZ-(TEV)-3×Flag-hTERT(WT)], [pCDNA6-ZZ-(TEV)-3×Flag- hTERT(DN)], or [pCDNA6-13×Myc-hTERT(WT)], and pBS-U1-hTR) as described[2] and whole-cell lysates (WCL) were prepared as described[3]. For telomerase affinity purification, the WCL was adjusted to a protein concentration of 4 mg/ml with buffer A (20 mM HEPES- KOH pH 7.9, 2 mM $MgCl_2$, 300 mM KCl, 10 % glycerol (v/v), 1 mM DTT, 1 mM EDTA, 0.1 % Triton X-100 (v/v), 1 mM PMSF) and clarified by filtration to produce the Input. To 20 ml Input 1 ml buffer A equilibrated IgG –Sepharose 6 Fast Flow (GE Healthcare #17-0969-01) was added and rotated for 3 hrs at 4°C and washed extensively with ice-cold buffer A. Telomerase was released from 1ml IgG –Sepharose by overnight incubation with 5 ml 0.05 mg/ml TEV protease (>90% efficient) in buffer A at 4°C. In a second affinity purification step, the soluble telomerase containing fraction was applied to a 1 ml HiTrap Heparin HP column (GE Healthcare #17-0406-01) previously equilibrated with buffer A and washed with 10 column volumes of buffer A to remove unbound proteins. Bound proteins were eluted using a gradient of 0.3 – 1 M KCl in buffer A. Fractions containing telomerase were identified using a direct telomerase activity assay (Fig. 1c) as described[3] and active fractions were pooled, concentrated, and dialyzed against buffer B (20 mM HEPES-KOH pH 7.9, 2 mM $MgCl_2$, 150 mM KCl, 10 % glycerol (v/v), 1 mM DTT, 1 mM EDTA, 1 mM PMSF). Telomerase yields were quantified by Northern blot analysis using hTR run-off transcripts as standards and the purity was assessed by SDS-PAGE.

Telomerase sucrose gradient sedimentation in combination with fixation (GraFix)

For EM analysis the telomerase complex was further purified using GraFix[4]. Briefly, solutions of buffer B containing 5 % and 30 % Sucrose were prepared in Falcon tubes. 0.1% glutaraldehyde (EM grade 25%, Science Services GmbH, Munich, Germany) was added to the high-density solution only. 4 ml gradients for centrifugation using a Beckman SW60 rotor were prepared using a gradient former (Gradient Master 107, BioComp Instruments, Canada). Freshly prepared gradients were kept at 4°C for one hr before sample loading. Subsequently 200 µl, containing 10-30 pmol of purified telomerase bound to 5′-[^{32}P]-$(TTAGGG)_2$-3′ was loaded on top of the gradient and run for 20 hr at max 215,000 × g and 4°C. Sucrose gradients were run in parallel without fixation reagent to assess whether the presence of glutaraldehyde caused any differences in particle sedimentation. 200 µl fractions were collected manually from top to bottom (Fig. 1b). The glutaraldehyde was inactivated after fractionation by adding glycine to a final concentration of 80 mM. For EM analysis, the sucrose from the GraFix fractions was removed by applying the sample to a buffer exchange spin column (Zeba spin columns, Pierce, Rockford, IL, USA) previously equilibrated with buffer C (20 mM Tris – HCl pH 7.6, 150 mM KCl, 1 mM $MgCl_2$).

SDS-PAGE and E MSA analysis

For SDS-PAGE analysis, 10 µl of extract were directly boiled for 5 min in Laemmli sample buffer and fractionated on a 4–20 % SDS–PAGE gradient gel. Proteins were silver stained. For the EMSA analysis, a two fold dilution series of IgG-Sepharose/Heparin purified telomerase fraction was incubated with 250 nM ^{32}P-$(TTAGGG)_3$ telomeric DNA in the presence of 5 µM CTAGACCTGTCATCA competitor DNA and 0.1 mg/ml acetylated BSA in heparin binding buffer (20 mM HEPES-KOH pH7.9, 300 mM KCl, 2 mM $MgCl_2$, 1 mM

EDTA pH8, 1 mM DTT, 10 % glycerol). Reactions were incubated at RT for 5 min before electrophoresis on a 6.7% acrylamide native gel (80:1 acrylamide:bis acrylamide, 5% glycerol, 0.5× Tris borate-EDTA) run at 200 V for 15 h at 4°C and fixed in MeOH/Acetate. As control, oligo DNA was incubated without telomerase. The gel was exposed to X-ray film.

Nano-liquid chromatography tandem mass spectrometry (nanoLC-MS/MS)

Analysis of the protein content of the purified telomerase samples was carried out by adding 20 μl of a trypsin solution (10 ng/μl in 10 mM Tris/2 mM $CaCl_2$, pH 8.2) to a 200-μl aliquot (estimated at 0.5 pmol) of the purified telomerase or control samples. Microwave (CEM Discover, CEM Corp., USA) assisted trypsin digestion was performed at 60°C at 5 W for 30 min. After digestion the sample was concentrated to approximately 50 μl in a vacuum centrifuge (Savant Instruments Inc., USA), diluted with 50 μl 0.1% formic acid and 4 μl was loaded onto a nano-UPLC system (nanoAcquity UPLC system, Waters, USA) through a trap-column (Symmetry, C18, 180 μm i.d. x 20 mm length, Waters, USA). Peptides were separated on a C18-column (BEH300 C18, 75 μm i.d. x 150 mm length, Waters, USA) at 250 nl/min using a linear gradient from 1 to 60% solvent B (solvent A: 0.1% formic acid in water, solvent B: 0.1% formic acid in acetonitrile) in 60 min. Mass spectra were recorded on a Synapt G2 HDMS (Waters, USA). Information-dependent data acquisition was carried out using a 0.5-second survey scan from which the five most abundant doubly and triply charged peptides were selected for product ion scans. The resulting data were searched against the SwissProt database using the ProteinLynx Global Server (Waters, USA) search engine (table S1).

Direct Telomerase Activity Assays

Conventional telomerase assays were carried out for 45 min at 30°C in 20-μl reactions containing 1 μl of cell extract, 50mM Tris– HCl (pH 8.0), 50mM KCl, 1mM spermidine, 1mM β-mercaptoethanol, 1mM $MgCl_2$, 0.5mM dATP, 0.5mM dTTP, 2 mM dGTP, 20 μCi of [α-^{32}P]dGTP (3000 Ci/mmol) and 1 μM of telomeric primer 5′-Biotin(T_2AG_3)-3′. Reactions were stopped by the addition of 5mM EDTA and 1% SDS. Biotinylated telomeric primers were recovered with Dynabeads® M-280 Streptavidin (Invitrogen) following the instructions provided by the manufacturer. Beads were re-suspended in 98% formamide containing 10mM EDTA and 0.005% xylene cyanol, heated to 95 °C for 5 min, and analyzed on a 12% polyacrylamide-urea sequencing gels.

Western analysis

For Western analysis, 4 μl of extract were boiled for 5 min in Laemmli sample buffer and fractionated on 4–15 % SDS–PAGE gradient gels. Immunoblots with standard protocols, using an affinity purified rabbit polyclonal antibody against hTERT (1:10000, R484) [5]. As secondary IRDye 800CW Goat anti-Rabbit IgG (Li Cor) was used (1:7000). The Li-Cor Infrared fluorescence detection of IRDye infrared dye substrate and imaging system was used to detect bound antibodies.

Telospot assay

Telospot telomerase activity assays were performed as previously described[6]. Briefly, telomerase activity reactions were carried out for 45 min at 30 °C in 20 μl volumes containing 1 μl of cell extracts, 50mM Tris– HCl (pH 8.0), 50mM KCl, 1mM spermidine, 1mM β-mercaptoethanol, 1mM $MgCl_2$, 33 μM dATP, 33 μM dTTP, 33 μM dGTP, and 0.25 mM of telomeric primer $(T_2AG_3)_3$. Reactions were stopped by the addition of 2 μl of 0.25M EDTA / 0.05% bromophenol blue solution. 0.5 μl of the reaction mix was spotted in quadruplicate on a GeneScreen Plus charged nylon membrane (PerkinElmer). DNA samples

were UV crosslinked to the membrane with the auto-crosslink function of a Stratalinker (Stratagene). Without prior denaturation membranes were blocked for 1 hr at 60 °C with church buffer. After overnight hybridization at 60 °C with a randomly labeled probe derived from a 600 bp TTAGGG-repeat containing DNA fragment, membranes were washed twice for 15 min with 2× SSC buffer at room temperature and twice for 30 min with 2× SSC, 0.1 % SDS at 65 °C and exposed to a phosphoimager screen. Spot intensities were quantified using 2D-densitometry and the Aida software (Raytest).

EM sample preparation and imaging

Continuous carbon-coated grids were freshly prepared and glow-discharged before use. 13 μl of telomerase sample (8-10 nM) were deposited on the grid for 15-30 minutes, blotted with filter paper and negatively stained with 2 drops of 1-2% (w/v) uranyl acetate solution. A homogenous sample preparation for EM was obtained using these conditions although the particle concentration was low (30-100 particles/image). Single particle EM data were collected on a FEI CM12 transmission electron microscope, operated at 120 keV and liquid nitrogen temperature. The nominal magnification was 42,000× (calibrated magnification, 42,550×). Micrographs were recorded on Kodak SO-163 film with an electron dose of 10-12 e/Å2 and a defocus of 1.0–1.5 μm. The films were developed in Kodak developer at full strength for 12 min and digitized with a Zeiss SCAI scanner using a step size of 7 μm. The micrographs were compressed x4 giving a final object pixel size of 6.6Å/pixel. Figures 1d and colloidal gold data were recorded on a 2k TVIPS CCD camera with an object pixel size of 3.25 Å. Single axis tilt series were recorded with SerialEM[7] on a FEI Tecnai G2 Polara microscope at 300keV and 3.5 μm underfocus. The specimen was tilted ±60° or ±65° and images were recorded every second degree on a 2k TVIPS CCD detector. The electron dose per image was 10 e/Å2 and the pixel size was 5.65 Å at the specimen level.

Particle selection and 2D class averaging

A data set of 26,361 telomerase particles bound to oligonucleotide 5′-$(TTAGGG)_2$- 3′ were selected manually with Ximdisp[8] using a box size of 78×78 pixels. The image stack was normalised and sorted by statistics in Xmipp[9], and 20,127 images were selected for further analysis. A maximum likelihood target function in Fourier space (MLF2D[10]) was used for multi-reference alignment and 2D classification.

Initial low-resolution 3D reconstruction by electron tomography

Electron tomography was used to calculate a low-resolution reference model. Single axis tilt series were compressed x2 giving a pixel size of 11.3 Å at the specimen level. The micrographs were coarsely aligned by cross-correlation and reconstructed by filtered back-projection in IMOD[11]. An iterative refinement procedure was used to refine the alignment parameters and the reconstruction in EMTIAR[12]. 50 evenly stained sub-tomograms corresponding to individual telomerase particles were manually selected in Bsoft[13] and extracted using a box size of 40×40×40 voxels. An average 3D reconstruction was calculated by missing-wedge weighted, reference-free alignment of sub-tomograms in Xmipp[14]. 13 sub-tomograms with the highest cross correlation to the average (Fig. 1f and fig. S3a) were included in the final sub-tomogram average.

Map refinement by single particle electron microscopy

Initial single-particle refinement was performed in EMAN2[15] using the sub-tomogram average (fig. S3a) as a starting reference. The reference model was initially filtered to 80 Å resolution and refined (fig. S3b) by 20 rounds of multi-reference alignment, classification by multivariate statistical analysis and angular assignment by projection matching. Class averages with 6 degree angular spacing were calculated using 6 averaging iterations. The 3D

structure was calculated at 35 Å resolution by direct Fourier inversion. To analyse structural variability in the telomerase dimer we used 3D-classification by maximum-likelihood in Fourier space (MLF3D[10]). After 25 rounds of non-supervised angular refinement against five reference models, four homogenous subsets of images were selected for further refinement (a fifth class was interpreted as an accumulation of particles of low quality). The selected classes contained 2608, 2631, 3659 and 5519 particles respectively. Subsequent refinement in EMAN2 (as described above) yielded reconstructions with resolutions in the range of 30-40 Å (fig. S3c-f).

Map validation and absolute hand determination

The absolute hand and the overall correctness of the dimer structure in Figure 3f were assessed using the tilt-pair validation method[16]. From one of the tilt series that was used to calculate electron tomograms for our reference-free initial model calculation, we selected the individual projections of one of the dimer particles (selection of other particles gave similar results). These single-particle projections were then aligned independently against reference projections of the dimer structure. Analysis of the relative tilt angles between these images (fig. S4) validated the structure, while comparison with an identical analysis for a tilt series that was collected on the same microscope on a sample of known handedness (helical assemblies of acetyl choline receptors) served to determine its absolute hand.

Independent monomer refinement and reconstruction of composite dimers

From 2D class averages of telomerase dimer side-views, we calculated the centre of each monomer in the raw image stack; 9,380 sub-images were selected of the open monomer and the closed monomer (4,690 each), and extracted using a box size of 34×34 pixels. These sub-images were used for independent monomer refinement, using a two-reference model procedure, in Xmipp (Fig. 4-5). To re-combine the monomers into composite dimers, reference-free 2D class averages (Fig. 4c top panel), were used to determine the orientation of the open and closed monomers (calculated as the average orientation of all sub-images that were included in the 2D class average). This analysis provided a reconstruction of the relative orientation of the independely refined monomers (Fig. 4c middle panel). Since the analysis was carried out using 2D class averages of side views, the Z-height of the monomers were adjusted by hand and compared to the previously refined intact dimer (Fig. 3f). Visual inspection shows that projections of the assembled composite dimer (Fig. 4c, lower panel) agreed well with the 2D class averages (Fig. 4c top panel).

Colloidal gold labeling of telomerase domains

Two types of 5 nm colloidal gold, coated with either streptavidin (prepared as described [17]) or Ni-NTA (Nanoprobes, Inc Yaphank, NY, USA), was used to identify the presence and location of the telomeric G-overhang and the TERT subunit respectively. The binding integrity of the monovalent streptavidin gold complex to 5′-[^{32}P]/biotin 5′-[^{32}P]-(TTAGGG)2-3′ -3′ was analysed by EMSA. After GraFix purification of the telomerase (as described above), streptavidin coated gold was added in a stochiometric ratio of 2:1 to telomerase bound to 5′- Biotin dT-(TTAGGG)$_2$- 3′ and incubated for 30 minutes on ice before preparing EM grids (Fig. 1g). To map the location of the TERT subunit, telomerase N-terminal 6×His-tag (ZZ_(TEV)_6×His_5x(AAAKE) ~37Å long alpha helix_3x_Flag_hTERT) was incubated with Ni-NTA coated gold for 3 hours at room temperature (Fig. 5d). We found more telomerase particles in complex with streptavidin coated gold (87%) compared to Ni-NTA coated gold (16%), which is likely to reflect the high affinity of streptavidin-biotin (not shown).

Model fitting and density visualization

The crystal structure of the TERT protein subunit (pdb code: 3KYL) was docked into the EM density of the monomeric subunit using automatic docking procedures in Chimera[18]. This program was also used for 3D density visualization and generating a 23 Å density map of the TERT subunit (Fig. S5b).

Supplementary Material

Refer to Web version on PubMed Central for supplementary material.

Acknowledgments

We are indebted to Patrick Reichenbach, Benoit Zuber, Steven J. Ludtke, Richard Henderson, Jude Short, Jake Grimmett, Shaoxia Chen and Alix Christen for help and advice. We thank Sarah Thurnheer and David Hacker (EPFL-PECF) for telomerase production and Peter Hunziker from the Functional Genomics Center Zurich for protein identification. We thank the Human Frontier Science Program for funding through a grant (number RGP0032/2005-C) awarded to J.L. and D.R. and a post-doctoral fellowship to A.S.. We thank the European Molecular Biology Organization for post-doctorial fellowships to A.S and S.S; the UK Medical Research Council for a career-development fellowship to S.S.. Work in J.L.'s laboratory is supported by the Swiss National Science Foundation and a European Research Council advanced investigator grant (grant agreement number 232812). Work in DR's and S.H.W.S.'s laboratory is supported by the UK Medical Research Council (MC_UP_A025_1013).

References

1. de Lange T. How telomeres solve the end-protection problem. Science. 2009; 326:948–952. [PubMed: 19965504]
2. Harley CB. Telomerase and cancer therapeutics. Nat Rev Cancer. 2008; 8:167–179. [PubMed: 18256617]
3. Greider CW, Blackburn EH. A telomeric sequence in the RNA of Tetrahymena telomerase required for telomere repeat synthesis. Nature. 1989; 337:331–337. [PubMed: 2463488]
4. Yu GL, Bradley JD, Attardi LD, Blackburn EH. In vivo alteration of telomere sequences and senescence caused by mutated Tetrahymena telomerase RNAs. Nature. 1990; 344:126–132. doi: 10.1038/344126a0. [PubMed: 1689810]
5. Cech T. Beginning to understand the end of the chromosome. Cell. 2004; 116:273–279. [PubMed: 14744437]
6. Lingner J, et al. Reverse transcriptase motifs in the catalytic subunit of telomerase. Science. 1997; 276:561–567. [PubMed: 9110970]
7. Blackburn EH, Collins K. Telomerase: an RNP enzyme synthesizes DNA. Cold Spring Harb Perspect Biol. 2011; 3
8. Weinrich S, et al. Reconstitution of human telomerase with the template RNA component hTR and the catalytic protein subunit hTRT. Nat Genet. 1997; 17:498–502. doi:10.1038/ng1297-4980. [PubMed: 9398860]
9. Autexier C, Lue N. The structure and function of telomerase reverse transcriptase. Annu Rev Biochem. 2006; 75:493–517. [PubMed: 16756500]
10. Cohen S, et al. Protein composition of catalytically active human telomerase from immortal cells. Science. 2007; 315:1850–1853. [PubMed: 17395830]
11. Egan E, Collins K. Specificity and stoichiometry of subunit interactions in the human telomerase holoenzyme assembled in vivo. Mol Cell Biol. 2010; 30:2775–2786. [PubMed: 20351177]
12. Venteicher A, et al. A human telomerase holoenzyme protein required for Cajal body localization and telomere synthesis. Science. 2009; 323:644–648. doi:10.1126/science.11653570. [PubMed: 19179534]
13. Errington TM, Fu D, Wong JM, Collins K. Disease-associated human telomerase RNA variants show loss of function for telomere synthesis without dominant-negative interference. Mol Cell Biol. 2008; 28:6510–6520. [PubMed: 18710936]

14. Wenz C, et al. Human telomerase contains two cooperating telomerase RNA molecules. EMBO J. 2001; 20:3526–3534. doi:10.1093/emboj/20.13.35260. [PubMed: 11432839]
15. Arai K, et al. Two independent regions of human telomerase reverse transcriptase are important for its oligomerization and telomerase activity. J Biol Chem. 2002; 277:8538–8544. Epub 2001 Dec 85180. [PubMed: 11751869]
16. Beattie TL, Zhou W, Robinson MO, Harrington L. Functional multimerization of the human telomerase reverse transcriptase. Mol Cell Biol. 2001; 21:6151–6160. [PubMed: 11509658]
17. Moriarty TJ, Huard S, Dupuis S, Autexier C. Functional multimerization of human telomerase requires an RNA interaction domain in the N terminus of the catalytic subunit. Mol Cell Biol. 2002; 22:1253–1265. [PubMed: 11809815]
18. Gardano L, Holland L, Oulton R, Le Bihan T, Harrington L. Native gel electrophoresis of human telomerase distinguishes active complexes with or without dyskerin. Nucleic Acids Res. 2011; 19:19.
19. Sekaran V, Soares J, Jarstfer M. Structures of telomerase subunits provide functional insights. Biochim Biophys Acta. 2010; 1804:1190–1201. doi:10.1016/j.bbapap.2009.07.0190. [PubMed: 19665593]
20. Wyatt H, West S, Beattie T. InTERTpreting telomerase structure and function. Nucleic Acids Res. 2010 doi:10.1093/nar/gkq370.
21. Zhang Q, Kim NK, Feigon J. Architecture of human telomerase RNA. Proc Natl Acad Sci U S A. 2011; 108:20325–20332. Epub 22011 Aug 203150. [PubMed: 21844345]
22. Mitchell M, Gillis A, Futahashi M, Fujiwara H, Skordalakes E. Structural basis for telomerase catalytic subunit TERT binding to RNA template and telomeric DNA. Nat Struct Mol Biol. 2010; 17:513–518. doi:10.1038/nsmb.17770. [PubMed: 20357774]
23. Schuller AP, Harkisheimer MJ, Skordalakes E. In vitro reconstitution of the active T. castaneum telomerase. J Vis Exp. 2011:e2799. doi: 2710.3791/27990. [PubMed: 21775967]
24. Kohlstaedt L, Wang J, Friedman J, Rice P, Steitz T. Crystal structure at 3.5 A resolution of HIV-1 reverse transcriptase complexed with an inhibitor. Science. 1992; 256:1783–1790. [PubMed: 1377403]
25. Gillis A, Schuller A, Skordalakes E. Structure of the Tribolium castaneum telomerase catalytic subunit TERT. Nature. 2008; 455:633–637. [PubMed: 18758444]
26. Jacobs S, Podell E, Cech T. Crystal structure of the essential N-terminal domain of telomerase reverse transcriptase. Nat Struct Mol Biol. 2006; 13:218–225. doi:10.1038/nsmb10540. [PubMed: 16462747]
27. Theimer C, Feigon J. Structure and function of telomerase RNA. Curr Opin Struct Biol. 2006; 16:307–318. doi:10.1016/j.sbi.2006.05.0050. [PubMed: 16713250]
28. Mitchell J, Collins K. Human telomerase activation requires two independent interactions between telomerase RNA and telomerase reverse transcriptase. Mol Cell. 2000; 6:361–371. [PubMed: 10983983]
29. Kelleher C, Teixeira M, Forstemann K, Lingner J. Telomerase: biochemical considerations for enzyme and substrate. Trends Biochem Sci. 2002; 27:572–579. [PubMed: 12417133]
30. Cristofari G, et al. Low- to high-throughput analysis of telomerase modulators with Telospot. Nat Methods. 2007; 4:851–853. [PubMed: 17893679]
31. Cristofari G, Lingner J. Telomere length homeostasis requires that telomerase levels are limiting. EMBO J. 2006; 25:565–574. [PubMed: 16424902]
32. Mitchell J, Wood E, Collins K. A telomerase component is defective in the human disease dyskeratosis congenita. Nature. 1999; 402:551–555. doi:10.1038/9901410. [PubMed: 10591218]
33. Howarth M, et al. A monovalent streptavidin with a single femtomolar biotin binding site. Nat Methods. 2006; 3:267–273. [PubMed: 16554831]
34. Hahn WC, et al. Inhibition of telomerase limits the growth of human cancer cells. Nat Med. 1999; 5:1164–1170. [PubMed: 10502820]
35. Kastner B, et al. GraFix: sample preparation for single-particle electron cryomicroscopy. Nat Methods. 2008; 5:53–55. [PubMed: 18157137]

36. Scheres SH, et al. Modeling experimental image formation for likelihood-based classification of electron microscopy data. Structure. 2007; 15:1167–1177. [PubMed: 17937907]
37. Rosenthal PB, Henderson R. Optimal determination of particle orientation, absolute hand, and contrast loss in single-particle electron cryomicroscopy. J Mol Biol. 2003; 333:721–745. [PubMed: 14568533]
38. Gardano L, Holland L, Oulton R, Le Bihan T, Harrington L. Native gel electrophoresis of human telomerase distinguishes active complexes with or without dyskerin. Nucleic Acids Res. 2012; 40:e36. Epub 2011 Dec 20190. [PubMed: 22187156]
39. Alves D, et al. Single-molecule analysis of human telomerase monomer. Nat Chem Biol. 2008; 4:287–289. [PubMed: 18391947]
40. Canudas S, et al. A role for heterochromatin protein 1gamma at human telomeres. Genes Dev. 2011; 25:1807–1819. Epub 2011 Aug 18240. [PubMed: 21865325]
41. Fouche N, Moon IK, Keppler BR, Griffith JD, Jarstfer MB. Electron microscopic visualization of telomerase from Euplotes aediculatus bound to a model telomere DNA. Biochemistry. 2006; 45:9624–9631. [PubMed: 16878997]
42. Nunez-Ramirez R, et al. Flexible tethering of primase and DNA Pol alpha in the eukaryotic primosome. Nucleic Acids Res. 2011; 39:8187–8199. Epub 2011 Jun 81280. [PubMed: 21715379]
43. Ren X, et al. Identification of a new RNA.RNA interaction site for human telomerase RNA (hTR): structural implications for hTR accumulation and a dyskeratosis congenita point mutation. Nucleic Acids Res. 2003; 31:6509–6515. [PubMed: 14602909]

References

1. Graham F, Smiley J, Russell W, Nairn R. Characteristics of a human cell line transformed by DNA from human adenovirus type 5. J Gen Virol. 1977; 36:59–74. [PubMed: 886304]
2. Cristofari G, et al. Human telomerase RNA accumulation in Cajal bodies facilitates telomerase recruitment to telomeres and telomere elongation. Mol Cell. 2007; 27:882–889. [PubMed: 17889662]
3. Cohen S, et al. Protein composition of catalytically active human telomerase from immortal cells. Science. 2007; 315:1850–1853. [PubMed: 17395830]
4. Kastner B, et al. GraFix: sample preparation for single-particle electron cryomicroscopy. Nat Methods. 2008; 5:53–55. [PubMed: 18157137]
5. Wenz C, et al. Human telomerase contains two cooperating telomerase RNA molecules. EMBO J. 2001; 20:3526–3534. doi:10.1093/emboj/20.13.3526. [PubMed: 11432839]
6. Cristofari G, et al. Low- to high-throughput analysis of telomerase modulators with Telospot. Nat Methods. 2007; 4:851–853. [PubMed: 17893679]
7. Mastronarde DN. Automated electron microscope tomography using robust prediction of specimen movements. J Struct Biol. 2005; 152:36–51. doi:10.1016/j.jsb.2005.07.007. [PubMed: 16182563]
8. Smith JM. Ximdisp--A visualization tool to aid structure determination from electron microscope images. J Struct Biol. 1999; 125:223–228. doi:10.1006/jsbi.1998.4073. [PubMed: 10222278]
9. Sorzano CO, et al. XMIPP: a new generation of an open-source image processing package for electron microscopy. J Struct Biol. 2004; 148:194–204. doi:10.1016/j.jsb.2004.06.006. [PubMed: 15477099]
10. Scheres SH, et al. Modeling experimental image formation for likelihood-based classification of electron microscopy data. Structure. 2007; 15:1167–1177. [PubMed: 17937907]
11. Kremer JR, Mastronarde DN, McIntosh JR. Computer visualization of three-dimensional image data using IMOD. J Struct Biol. 1996; 116:71–76. [PubMed: 8742726]
12. Chen H, Hughes DD, Chan TA, Sedat JW, Agard DA. IVE (Image Visualization Environment): a software platform for all three-dimensional microscopy applications. J Struct Biol. 1996; 116:56–60. [PubMed: 8742723]
13. Heymann JB, Belnap DM. Bsoft: image processing and molecular modeling for electron microscopy. J Struct Biol. 2007; 157:3–18. [PubMed: 17011211]

Europe PMC Funders Author Manuscripts

14. Scheres SH, Melero R, Valle M, Carazo JM. Averaging of electron subtomograms and random conical tilt reconstructions through likelihood optimization. Structure. 2009; 17:1563–1572. [PubMed: 20004160]
15. Tang G, et al. EMAN2: an extensible image processing suite for electron microscopy. J Struct Biol. 2007; 157:38–46. doi:10.1016/j.jsb.2006.05.009. [PubMed: 16859925]
16. Rosenthal PB, Henderson R. Optimal determination of particle orientation, absolute hand, and contrast loss in single-particle electron cryomicroscopy. J Mol Biol. 2003; 333:721–745. [PubMed: 14568533]
17. Beesley, JE. Colloidal gold : a new perspective for cytochemical marking. Oxford University Press [for] Royal Microscopical Society; 1989. p. 17Vol. Microscopy handbooks
18. Pettersen EF, et al. UCSF Chimera--a visualization system for exploratory research and analysis. J Comput Chem. 2004; 25:1605–1612. doi:10.1002/jcc.20084. [PubMed: 15264254]

Europe PMC Funders Author Manuscripts

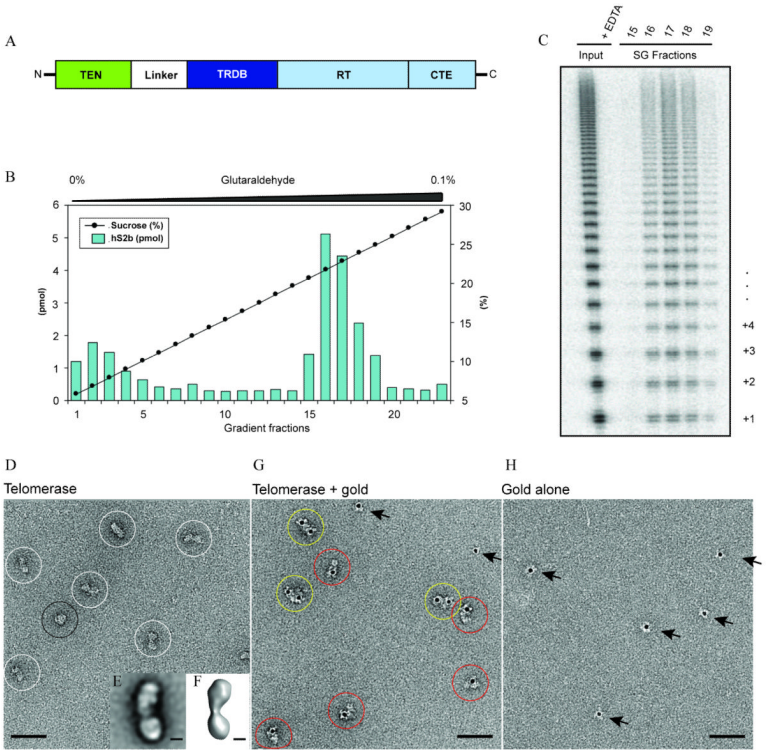

Figure 1. Human telomerase is a dimer

a, Schematic of hTERT domain arrangement: The essential N-terminal domain involved in DNA binding (TEN), the RNA binding domain (TRBD), the reverse transcriptase domain (RT) that contains the catalytic site and the C-terminal extension (CTE). **b**, Elution profile of the *in vivo* assembled human telomerase in complex with the G-overhang oligonucleotide 5′-[^{32}P]/biotin dT](TTAGGGT)$_2$-3′ fractionated on a sucrose gradient. **c**, Telomerase activity profile of a telomerase sample fractionated as in (b), but in the absence of G-overhang. G-overhang bound (b) and unbound (c) telomerase complexes migrate in the same position on the sucrose gradient. **d,** Electron micrograph of negatively stained telomerase bound to the G-overhang. Top views are indicated by black circles and side views by white circles. **e,** Example of reference-free 2D class averages. **f,** 3D structure obtained by subtomogram averaging. **g and h,** Electron micrographs of telomerase bound by 5 nm colloidal gold coated with streptavidin **(g)** and 5 nm colloidal gold coated with streptavidin in the absence of telomerase **(h)**. Telomerase dimers in complex with one gold particle are circled in red and in complex with two gold particles circled in yellow. The arrows indicated colloidal gold particles that are not bound to telomerase. The scale bar in images **(d)**, **(g) and (h)** is 50 nm and in images **(e)** and **(f)** is 5nm.

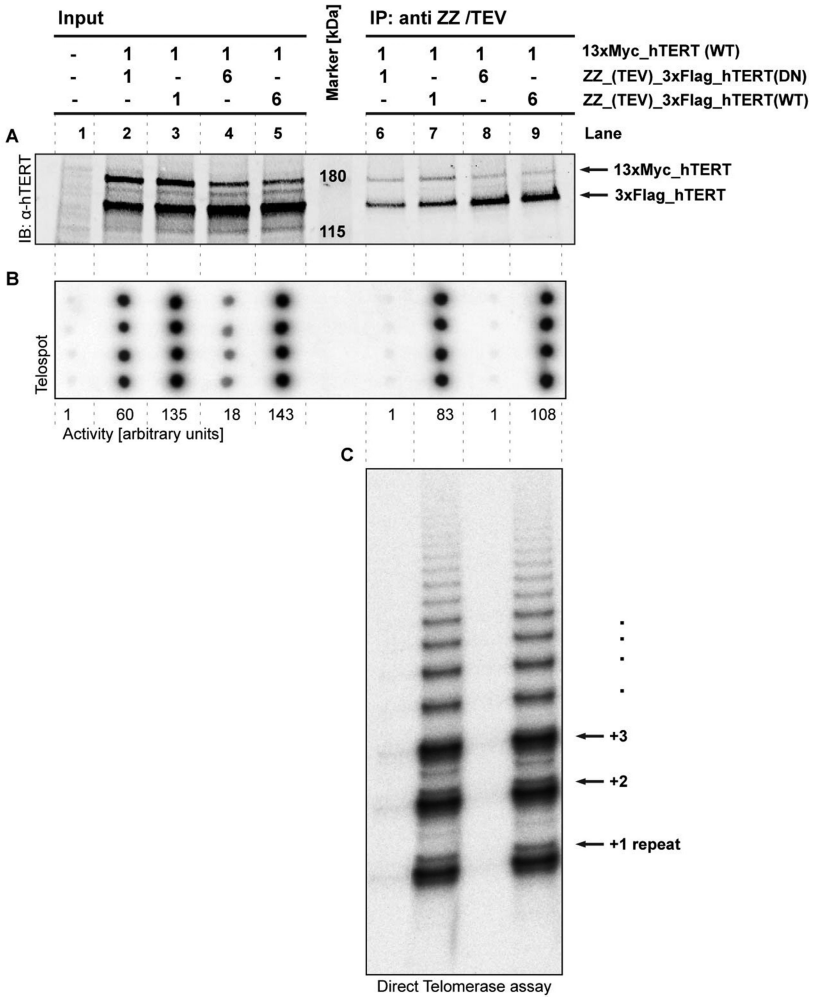

Figure 2. Active human telomerase functions as a dimer

Expression plasmids 13×Myc hTERT (WT) and hTER (WT) were transiently co-expressed in HEK293T cells together with either ZZ 3×Flag hTERT(WT), or the catalytically dead mutant ZZ 3×Flag hTERT(DN) at the ratios indicated at the top of the figure. **a,** Western blot analysis using an anti C-terminal hTERT antibody of TEV protease treated input whole cell lysates (left panel) and immunoaffinity purified and TEV protease released telomerase complexes (right panel). Whole cell lysate of untransfected HEK 293T cells was used as an expression control. For the left panel, the intensity of the TERT subunit is consistent with input expression plasmids. For the right hand panel showing the affinity purified and TEV released complexes, the intensities of the bands are consistent with the release of Flag_hTERT-Flag_hTERT dimers and Myc_hTERT-Flag_hTERT dimers, or Myc_hTERT-Flag_hTERT (DN) dimers **b**, Telospot telomerase activity assay of input whole cell lysate (left panel) and immunoaffinity purified and TEV released telomerase complexes (right panel). Telomerase activity in the transfected cells is shown as a multiple of the telomerase activity measured for untransfected HEK293T whole cell lysate. **c**, Direct telomerase activity assay of the immunoaffinity-purified and TEV released telomerase complexes. The presence of mutant hTERT (DN) has a dominant negative effect on telomerase activity.

Europe PMC Funders Author Manuscripts

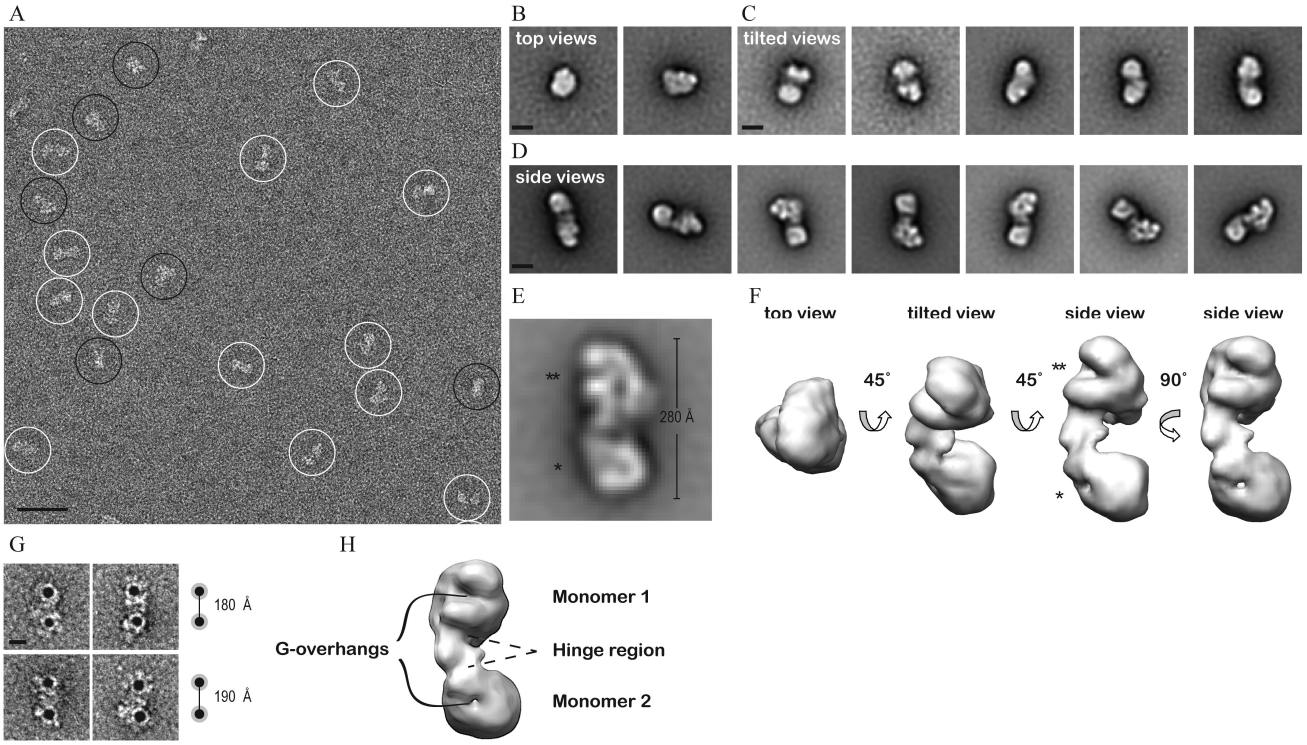

Figure 3. Analysis of the telomerase dimer by single-particle EM

a, Field view of negatively stained telomerase dimers with individual particles circled in black (top and tilted views) and white (side views). **b-d**, Examples of reference-free 2D class averages with representative top views, tilted views and side views as indicated. **f,** Examples of 2D class averages (also shown in movie S1), in which the two monomers in the dimer exhibit considerable differences in their relative orientations. The double star (**) indicated the V-shaped opening in the top monomer and the single star (*) the closed view of the lower monomer. **f,** Four views of a refined dimer density map after MLF3D classification. The relative rotations are indicated **g**, Individual telomerase dimers in complex with biotinylated $(TTAGGG)_2$ bound to two streptavidin coated gold particles. The distance between the two gold particles in the dimer is 180-190Å. **h,** The locations of the two G-overhang binding site and the hinge region are shown on the structure of the dimer. The scale bar in image **(a)** 50nm and in images b-d,g) 10 nm.

Europe PMC Funders Author Manuscripts

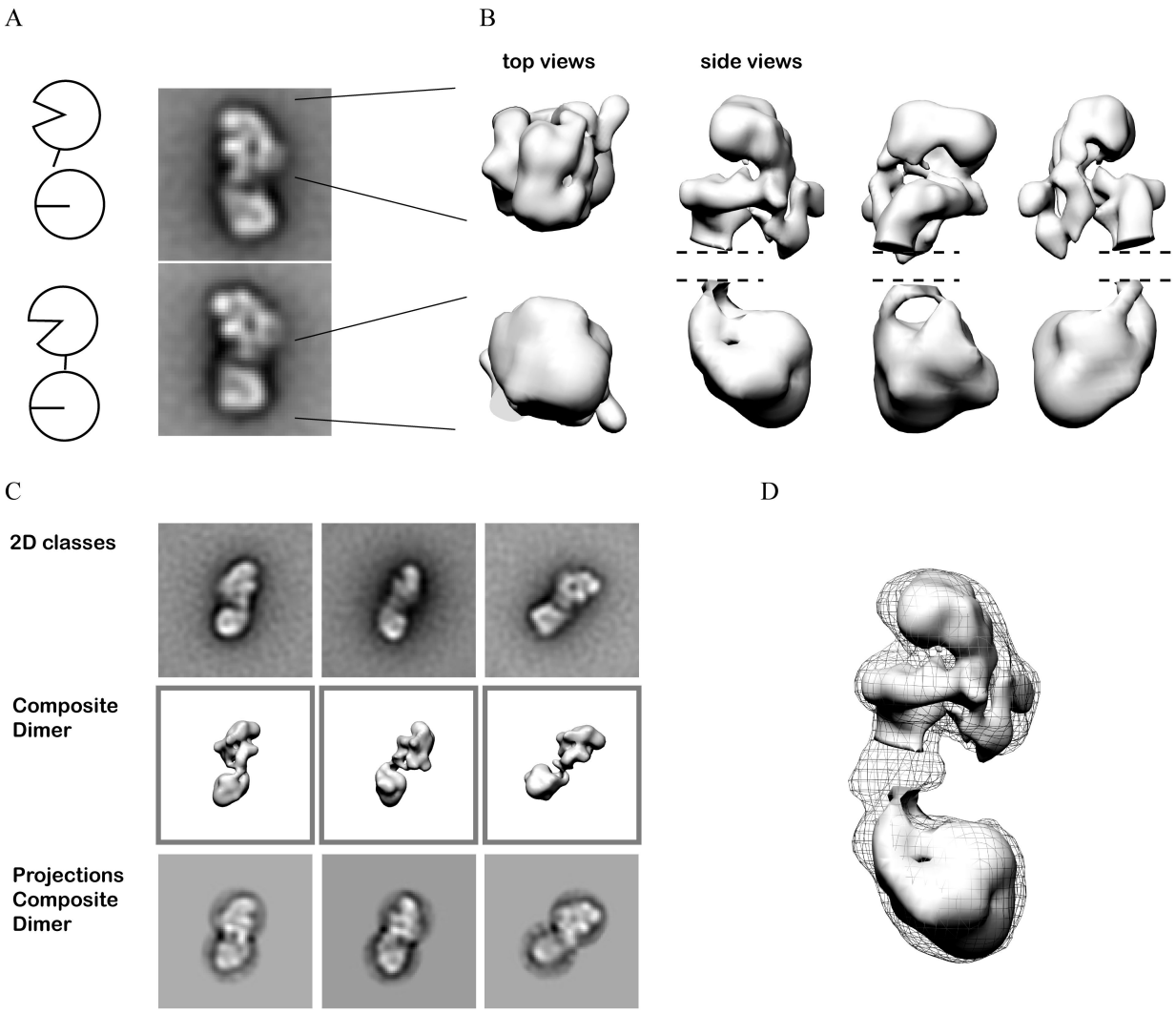

Figure 4. Independently refined monomers and composite dimers

a, The left panels indicate the boxed out areas used for the independent refinement of both the open and closed monomer. **b)** Four views of the open monomer (upper panel) and closed monomer (lower panel), in which the side views are related by a 90° rotation around the horizontal axis. **c,** Comparison of three 2D class averages (top panel) from which three composite dimers were reconstructed (middle panel) and the corresponding projections (lower panel). **d)** Surface rendered refined monomer reconstructions (non-transparent) placed within the EM density of the telomerase dimer density (wire frame).

Europe PMC Funders Author Manuscripts

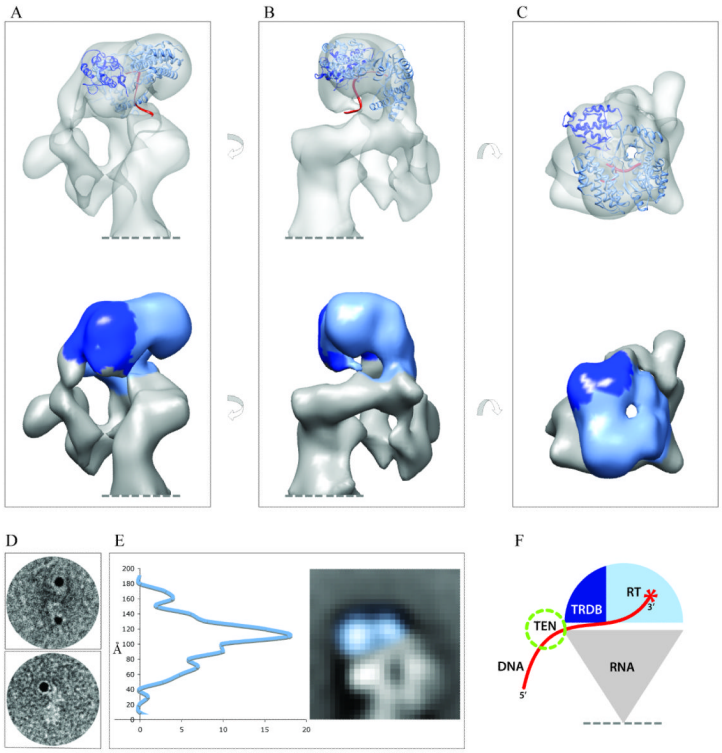

Figure 5. Assignment of the TERT and TER subunit within the 3D map of the open telomerase monomer

a-c, Three views of the three-dimensional map of the telomerase refined monomer into which the crystal structure of the beetle TERT subunit has been fitted. The upper panels show the EM density in transparent surface representation, together with the docked crystal structure. The lower panels show the EM density in non-transparent surface rendering. View (a) and (b) are related by a 90° rotation around the vertical axis. View (b) and (c) are related by a 90° rotation around the horizontal axis. Light blue depicts the RT domain; dark, blue the TRDB domain and red the DNA strand in the catalytic site. **d**, Electron micrographs of individual negatively stained telomerase containing His-tagged TERT subunit in complex with Ni-NTA-5nm colloidal gold. **e**, Distribution plot showing the distance between the Ni-NTA-gold and the dimer interface (y-axis), and the number of gold particles (x-axis). Although the large size of the gold particles complicates the analysis to some extent, a pronounced peak at 110 Å is in good agreement with the proposed location of TERT (blue) in the EM density map (a-c). **f**, Cartoon representation showing the interpretation of the EM density map. The colour coding for TERT is as in (a). A tentative location of the TEN domain is shown in green. Grey depicts the TER subunit, and the dotted line indicates the dimer interface.